

1 **Longitudinal and seasonal variations in plasmaspheric electron density:**  
2 **Implications for electron precipitation.**

3  
4 M. A. Clilverd, N. P. Meredith, R. B. Horne, S. A. Glauert

5 British Antarctic Survey,

6 Natural Environment Research Council,

7 Madingley Road, Cambridge, CB3 0ET, England.

8 [macl@bas.ac.uk](mailto:macl@bas.ac.uk), [nmer@bas.ac.uk](mailto:nmer@bas.ac.uk), [rh@bas.ac.uk](mailto:rh@bas.ac.uk), [sagl@bas.ac.uk](mailto:sagl@bas.ac.uk)

9  
10 R. R. Anderson,

11 Department of Physics and Astronomy,

12 The University of Iowa, Iowa City, Iowa, IA 52242-1479.

13 [roger-r-anderson@uiowa.edu](mailto:roger-r-anderson@uiowa.edu)

14  
15 N.R. Thomson

16 Department of Physics,

17 University of Otago,

18 Dunedin, New Zealand.

19 [n\\_thomson@physics.otago.ac.nz](mailto:n_thomson@physics.otago.ac.nz)

20  
21  
22 F. W. Menk,

23 Department of Physics,

24 University of Newcastle,

25 Newcastle, NSW

26 Australia

27 [Fred.Menk@newcastle.edu.au](mailto:Fred.Menk@newcastle.edu.au)

28  
29 B. R. Sandel,

30 Lunar and Planetary Laboratory,

31 The University of Arizona,

32 Sonett Space Sciences Building,

33 1541 East University Boulevard,

34 Tucson,

35 AZ 85711-0063, U.S.A.

36 [sandel@arizona.edu](mailto:sandel@arizona.edu)

37  
38 Abstract: The tilt and offset of the Earth's magnetic field can significantly affect the

39 longitudinal and seasonal distribution of electron density in the plasmasphere. Here

40 we show that for the solar maximum conditions of 1990-91, the largest annual

41 variation determined from CRRES measurements of plasmaspheric equatorial

42 electron density in the range  $L=2.5-5.0$  occurs at American longitudes ( $-60^\circ\text{E}$ ), while

43 no annual variation occurs at Asian longitudes ( $+100^\circ\text{E}$ ). Plasmaspheric electron

44 density is larger in December than in June at most longitudes, from  $-180^\circ\text{E}$  eastwards

45 to +20°E. At all other longitudes the density ratio from December to June is very  
46 close to 1.0. The largest December/June density ratio is at L=3.0 at American  
47 longitudes (-60°E). At L=4.5 and above, the annual variation disappears. The lowest  
48 electron density values for a given L-shell occur at American longitudes, in June. Ion  
49 densities also show significant annual variations, with similar longitudinal and  
50 seasonal characteristics in the case of IMAGE EUV He<sup>+</sup> measurements. Atomic mass  
51 density measurements calculated using the magnetometer cross-phase technique show  
52 significant seasonal variations, but also imply composition changes with longitude.  
53 Using the quasilinear PADIE code we calculate the bounce-averaged diffusion rate of  
54 electrons by plasmaspheric hiss with a fixed wave intensity. December to June  
55 variations in plasmaspheric density, particularly at American longitudes, drive  
56 changes in the wave-particle interactions, increasing diffusion into the loss cone by a  
57 factor of ~3 at 1 MeV at L=3.0, thus hardening the electron precipitation spectrum  
58 during the southern hemisphere winter (in June).  
59

59 Introduction

60

61 The plasmasphere is a region of low energy ('cold' i.e.,  $T_e \sim 1$  eV) plasma  
62 surrounding the Earth, and extending out to  $L \sim 2-6$  depending on geomagnetic  
63 latitude, geomagnetic disturbance levels, and on local time. It is primarily made up of  
64 electrons and protons that have diffusively migrated from the underlying ionosphere.  
65 Overlapping the plasmasphere are regions of high energy ('hot' i.e.,  $T_e \sim 1$  MeV)  
66 plasma known as the radiation belts. Low frequency radio waves propagating within  
67 the plasmasphere can interact with the high energy radiation belt particles, changing  
68 their energy spectra and causing them to precipitate into the Earth's upper  
69 atmosphere, driving chemical changes [e.g., Rosanov et al., 2005]. Variability in the  
70 background conditions of the plasmasphere is one of the factors in determining the  
71 efficiency of wave-particle interactions [e.g., Horne et al., 2003], thus influencing the  
72 resultant particle precipitation into the atmosphere. Here we use CRRES satellite  
73 measurements of 'cold' plasmaspheric equatorial electron density to investigate the  
74 longitudinal and annual variations in density in the range  $L=2.5-5.0$ , and assess the  
75 effect on the rate of 'hot' electron precipitation from the overlapping outer radiation  
76 belt.

77

78 The annual variation in equatorial plasmaspheric electron density ( $N_{eq}$ ) has been  
79 observed previously. The first observations were made using natural whistler signals,  
80 typically at either American or European longitudes [e.g., Helliwell, 1965; Park et al.,  
81 1978; Tarcsai et al., 1988]. In these cases  $N_{eq}$  showed a maximum in December and a  
82 minimum in June, with December larger by a factor of between 1.5-3.0 at  $L=1.5-2.5$ ,  
83 depending on longitude.

84

85 Man-made whistler-mode signals from US Naval transmitters were analysed by  
86 Clilverd et al. [1991] and showed a December to June ratio of Neq of 3.0 (2.0) at solar  
87 minimum (maximum) at L=2.5 in the American longitude sector, and a ratio of 1.4 at  
88 solar maximum in the New Zealand/Pacific longitude sector. Using conjugate  
89 ionosonde pairs such as Wallops Island (37.9°N, 75.5°W, L=2.39) and Argentine  
90 Islands (65.3°S, 64.3°W, L=2.44) Clilverd et al. [1991] showed that the seasonal Neq  
91 variation was largest at 300°E geographic (-60°E) because at that longitude the offset  
92 of the geomagnetic field configuration relative to geographic coordinates is largest.  
93 Calculations showed that each field line flux tube is in long-term diffusive  
94 equilibrium with the underlying ionospheres at the footprints of the field line and the  
95 annual behaviour of the plasmasphere reflects the local annual variation of the  
96 northern and southern F2 regions linked to it. In Figure 1 we show this variation of the  
97 geographic latitude of the footprints of the L=2.5 field line contour, using the IGRF  
98 magnetic field model, as a function of geographic longitude. The southern L=2.5  
99 contour at -60°E has an underlying ionosphere that is at high latitude and thus  
100 continually sunlit during the December solstice, and in near continuous darkness  
101 during the June solstice. These factors, along with differing horizontal thermospheric  
102 winds at such high geographic latitudes driving the ionospheric plasma up the field  
103 lines, produce significant changes in plasmaspheric density from solstice to solstice.  
104 Clilverd et al. [1991] also suggested that there would be no annual variation at  
105 African/Asian longitudes, and that in June global Neq values at L=2.5 would be  
106 largely independent of longitude and similar to that observed at -60°E, i.e., ~1000  
107 el.cm<sup>-3</sup>.

108

109 The annual variation in Neq has been modelled with a view to reproducing the  
110 observations, and understanding the underlying physical processes responsible. Some  
111 models reproduced the December/June annual variation at American longitudes, and  
112 then made predictions regarding the effect at other longitudes. Early work by  
113 Rasmussen and Schunk [1990] showed a Neq maximum in June rather than December  
114 as is actually observed – probably because of the centred dipole model used.  
115 Modelling work undertaken by Rippeth et al. [1991], which included a tilted offset  
116 dipole in the model, was better able to reproduce the observations at L=2.5 at  
117 American longitudes. Guiter et al. [1995] modelled plasmaspheric densities at L=2  
118 and found that Neq was 1.5 times higher in December than in June for 300°E (-60°E)  
119 longitude. At 120°E longitude the L=2 Neq was predicted to be higher in June than  
120 December by a factor of 1.2. The underlying mechanism driving the annual variation  
121 was considered to be variations in ionospheric O<sup>+</sup>.

122

123 Further modelling using the field line interhemispheric model (FLIP) indicated that  
124 the annual variation at American and Australian longitude sectors were likely to be 6  
125 months out of phase [Richards et al., 2000]. This work concluded that plasmaspheric  
126 thermal structure, not ionospheric density, should play a key role in producing the  
127 annual variation at solar minimum. A new approach using dynamical diffusive  
128 equilibrium, called the global plasmasphere ionosphere density model (GPID), was  
129 able to reproduce the observed seasonal variations in Neq at L=2.5 during solar  
130 maximum, but not at solar minimum [Webb and Essex, 2001].

131

132 To maintain charge neutrality an annual variation in ion concentration would be  
133 anticipated. Berube et al. [2003] used data from a pair of magnetometers at L=1.74 in

134 the MEASURE array (American longitudes) to determine the plasmaspheric  
135 equatorial mass density. They observed an annual variation in mass density with  
136 December densities 2-3 times higher than in June. This suggests that the mass  
137 densities vary in a similar way to the electron densities. Although at  $L < 2$ , the annual  
138 variation in field line resonance frequencies is due to the influence of  $O^+$  in the  
139 underlying ionosphere changing the Alfvén speed profile along those flux tubes  
140 [Waters et al., 1994].

141

142 Here we perform a comprehensive study of the longitudinal and seasonal variation  
143 of the equatorial plasmaspheric electron density in the region  $2.5 < L < 5.0$  using data  
144 from the CRRES satellite. We examine the observed  $N_{eq}$  radial profiles during solar  
145 maximum conditions (1990/91) at different longitudes and at different times of year,  
146 and compare the profiles against the commonly used profiles of Carpenter and  
147 Anderson, 1992. We also investigate the equivalent mass density variations using the  
148 IMAGE EUV measurements of  $He^+$ , and atomic mass from the cross-phase analysis  
149 of ground-based magnetometer data. The relevance of the plasmaspheric density  
150 variations are put into the context of changing wave-particle interactions, and the  
151 subsequent deposition of energetic particles into the upper atmosphere.

152

153

153

154

155 Determination of electron densities in the plasmasphere

156

157 Electron number densities are derived from wave data provided by the Plasma Wave

158 Experiment on board the Combined Release and Radiation Effects Satellite (CRRES).

159 This satellite, which was launched on 25 July 1990, operated in a highly elliptical

160 geosynchronous transfer orbit with a perigee of 305 km, an apogee of 35,768 km and

161 an inclination of 18°. The orbital period was approximately 10 hours, and the initial

162 apogee was at a magnetic local time (MLT) of 0800 MLT. The magnetic local time of

163 apogee decreased at a rate of approximately 1.3 hours per month until the satellite

164 failed on 11 October 1991, when its apogee was at about 1400 MLT. The satellite

165 swept through the plasmasphere on average approximately 5 times per day for almost

166 15 months. The Plasma Wave Experiment provided measurements of electric fields

167 from 5.6 Hz to 400 kHz, using a 100 m tip-to-tip long wire antenna, with a dynamic

168 range covering a factor of at least  $10^5$  in amplitude [Anderson et al., 1992].

169

170 The sweep frequency receiver, which is used in this study, covered the frequency

171 range from 100 Hz to 400 kHz in four bands with 32 logarithmically spaced steps per

172 band, the fractional step separation being about 6.7% across the entire frequency

173 range. Band 1 (100 Hz to 810 Hz) was sampled at one step per second with a

174 complete cycle time of 32.768 s. Band 2 (810 Hz to 6.4 kHz) was sampled at two

175 steps per second with a complete cycle time of 16.384 s. Band 3 (6.4 to 51.7 kHz) and

176 band 4 (51.7 kHz to 400 kHz) were sampled 4 times per second with complete cycling

177 times of 8.192 s.

178 The electron number density is determined from the electron plasma frequency,  $f_{pe}$ ,  
179 using the standard expression  $n_e = 4\pi^2 f_{pe}^2 \epsilon_0 m_e / e^2$ . When emissions at the upper hybrid  
180 frequency,  $f_{uhr}$ , are well-defined the electron plasma frequency,  $f_{pe}$ , is derived from  $f_{uhr}$   
181 using the relationship  $f_{pe}^2 = f_{uhr}^2 - f_{ce}^2$ , where  $f_{ce}$  is the electron gyrofrequency,  
182 determined from the CRRES fluxgate magnetometer [Singer et al., 1992]. When the  
183 upper hybrid frequency cannot be identified the electron plasma frequency is  
184 estimated from the lower frequency limit of the electromagnetic continuum radiation,  
185 which is taken to be the plasma wave cutoff at the plasma frequency [Gurnett and  
186 Shaw, 1973]. The number densities are initially determined at a temporal resolution of  
187 8.192 s and subsequently averaged as a function of half orbit (inbound or outbound)  
188 and L in steps of 0.1L. The position of the CRRES spacecraft is mapped to the  
189 ionosphere at the same temporal resolution using the IGRF 85 model corrected for  
190 external magnetospheric currents by the Olson-Pfizer tilt dependent static model  
191 [Olson and Pfizer, 1977]. This is the standard process used to analyze all CRRES  
192 data. The geographic coordinates are then averaged as a function of half orbit and L  
193 shell in steps of 0.1L. The time in UT, magnetic latitude, magnetic local time and time  
194 spent in each bin are also recorded at the same resolution.

195

196 The resulting database is subsequently analysed to determine the behaviour of the  
197 plasmaspheric equatorial number density as a function of geographic longitude and  
198 for different L shells and seasons. Throughout this paper we use geographic longitude  
199 during discussions of the results and the figures shown. We focus on periods centred  
200 near the solstices and use the data from October to February (inclusive) for the  
201 December solstice and from April to August (inclusive) for the June solstice. For each  
202 season the data are averaged into bins that are  $5^\circ$  in geographic longitude for L shells

203 ranging from 2.5 +/- 0.3 L to 5.0 +/- 0.3 L in steps of 0.5L. The data are included in  
204 the averaging process only when the measurements are made within the plasmasphere  
205 and when the magnetic latitude of the CRRES spacecraft lies within +/- 10° of the  
206 magnetic equator.

207

208 Data are selected to be in the plasmasphere using a criterion based on the amplitude  
209 of the waves in the frequency band  $f_{ce} < f < 2f_{ce}$ . Waves in this frequency band, which  
210 contains contributions from both electron cyclotron harmonic waves and thermal  
211 noise, tend to be excluded from the high density region inside the plasmopause.  
212 Specifically observations in the plasmasphere are identified using the criterion that the  
213 wave amplitude for frequencies in the range  $f_{ce} < f < 2f_{ce}$  must be less than 0.0005  
214  $\text{mV m}^{-1}$  [Meredith et al., 2004]. Observations made in regions where this criterion did  
215 not hold are assumed to be outside the plasmopause at the time and are excluded from  
216 the analysis. In practice although we exclude data during large geomagnetic storms  
217 using the wave amplitude criterion we will include some density values when the  
218 plasmasphere is likely to be in an intermediate refilling state following the storms.  
219 Overall, our criterion for selecting plasmaspheric measurements is somewhat  
220 conservative in that we reject ~14% of the data where the ECH waves in the range  $f_{ce}$   
221  $< f < 2f_{ce}$  have amplitudes above 0.0005  $\text{mV m}^{-1}$  but the densities are likely to be  
222 representative of the plasmasphere at the time [Meredith et al., 2004]. However, this  
223 criterion does reduce the number of low density measurements included in our  
224 analysis where the plasmopause is ill-defined, and when the plasmasphere is subject to  
225 erosion during geomagnetically active periods (i.e.,  $\text{AE} > 100 \text{ nT}$ ).

226

227 Determination of ion densities in the plasmasphere

228

229           The ion mass densities presented in this study were calculated using field-line  
230 resonant frequencies (FLRs) measured from pairs of ground-based magnetometers,  
231 following the analytical expressions described by Taylor and Walker [1984] and  
232 Walker et al. [1992]. These assume decoupled toroidal mode oscillations and yield  
233 essentially identical results to the models described by Orr and Matthew[1971].  
234 Techniques for the detection of FLRs were summarized by Menk et al. [1999] and  
235 Menk et al. [2000]. When examining data from latitudinally-separated  
236 magnetometers, the resonant frequency is identified by the peak in H-component  
237 cross-power and cross-phase, and a unity crossing in H-component power ratio,  
238 approximately mid-way between the stations. Where only one station is available the  
239 resonance is indicated by a peak in the power ratio H/D and a rapid change in  
240 polarization i.e., in the phase between the H and D components.

241

242           The uncertainty in our calculated mass densities presented in this study (20-  
243 30%) depends mainly on uncertainty in the frequency measurement with uncertainties  
244 typically of order 10-15%. Menk et al. [1999] discussed the relationship between  
245 these two uncertainties and found the mass density uncertainty to be typically double  
246 the uncertainty in frequency measurement. We have assumed a dipole magnetic field,  
247 and at L=2.5 this introduces negligible error.

248

249           Measurements of the He<sup>+</sup> ion density presented in this study were made with  
250 the Extreme Ultraviolet Imager (EUV Imager) on-board the IMAGE spacecraft, by  
251 detecting its resonantly-scattered emission at 30.4 nm [Sandel et al., 2001]. The  
252 IMAGE spacecraft is in an elliptical polar orbit with an apogee altitude of 7.2 Earth

253 radii (46,000 km) and a perigee altitude of 1,000 km, and completes one orbit every  
254 14.2 hours. Effective imaging of the plasmaspheric He<sup>+</sup> requires global 'snapshots' in  
255 which the high apogee and the wide field of view of the EUV Imager provide in a  
256 single exposure a map of the entire plasmasphere. The 30.4 nm feature is relatively  
257 easy to measure because it is the brightest ion emission from the plasmasphere, it is  
258 spectrally isolated, and the background at that wavelength is negligible. Line-of-sight  
259 measurements are easy to interpret because the plasmaspheric He<sup>+</sup> emission is  
260 optically thin, so its brightness is directly proportional to the He<sup>+</sup> column abundance.  
261 The EUV Imager instrument consists of three identical sensor heads, each having a  
262 field of view of 30°. These sensors are tilted relative to one another to cover a fan-  
263 shaped field of 84° x 30° that is swept across the plasmasphere by the spin of the  
264 satellite. EUV Imager's spatial resolution is ~0.6° or ~0.1 Re in the equatorial plane  
265 seen from apogee. The sensitivity is sufficient to map the position of the plasmopause  
266 with a time resolution of 10 minutes or better.

267

268         For this study we selected EUV measurements from times in June and  
269 December 2001. We used 122 images taken from the period 15-17 June and 97  
270 images from the period 9-20 December. All images were from quiet times ( $K_p \leq 2$ ),  
271 chosen to avoid azimuthal structures that often appear during more active times. After  
272 transforming each image to the plane of the magnetic equator [Sandel et al., 2003]  
273 using magnetic longitude as the azimuthal coordinate, we summed the images to a  
274 single image for each of June and December. The summation omitted the region of  
275 Earth's shadow and the overlaps between the three EUV cameras.

276

277 We derived azimuthal profiles of brightness vs. magnetic longitude by  
278 sampling these composite images in an annulus of width  $0.3 L$  centered at  $L=2.5$  with  
279 a bin size of  $5^\circ$  in magnetic longitude. To infer equatorial  $\text{He}^+$  abundances from the  
280 measured brightness, we used the concept of effective path length described by  
281 Clilverd et al. [2003] and Gallagher et al. [2005].

282

283 Longitudinal and seasonal variations in plasmaspheric densities

284

285 Figure 2 shows the density variation with longitude from CRRES for December  
286 (solid line) and June (dashed line) for  $L=2.5-5.0$ . Some of the data shown for  
287 December at  $L=2.5$  are indicated by a dot-dashed line, indicating that they are less  
288 reliable than the other data. The densities at these longitudes in December were so  
289 large ( $>2000 \text{ el. cm}^{-3}$ ) that the upper hybrid frequency could not be determined at all  
290 times, and data from a higher range of L-shells ( $L=2.7-3.3$ ) were used and linearly  
291 extrapolated to  $L=2.5$  and shown as the dot-dashed line. Thus the data should be  
292 treated as less reliable than the rest shown. However, the same extrapolation  
293 technique used on the  $L=2.5$  June data, and some of the other panels ( $L=3.0-4.0$ )  
294 reproduced the December data to within 5%. We make this extrapolation for the  
295  $L=2.5$  December data primarily to allow comparison with previous work, it does not  
296 materially affect any of the conclusions from this paper.

297

298 For  $L=2.5-3.5$  it is clear that the density is much higher in December than June over  
299 the longitude range  $-180^\circ\text{E}$  to  $20^\circ\text{E}$ . At the remaining longitudes the December and  
300 June densities are much more nearly equal, with occasionally the June densities  
301 exceeding the December ones by up to 10%. The same relationship occurs for the

302 higher L-shell regions ( $L \sim 4.0$ ), although the data are more sparse because of  
303 incursions by the plasmopause and hence the plots are somewhat less clear. As  
304 expected the average density level decreases with increasing L-shell as the plasma  
305 from the underlying ionosphere diffuses up into ever increasing flux tube volumes.  
306 This is true for each season, and every longitude.

307

308 The largest difference in density between December and June occurs at about  $-60^\circ\text{E}$   
309 longitude, which is consistent with the conclusions of Clilverd et al. [1991]. At  $L=2.5$   
310 the densities in June at this longitude are  $\sim 1000 \text{ el.cm}^{-3}$ , while the December densities  
311 are  $\sim 2500 \text{ el.cm}^{-3}$ . This compares well with the whistler-mode results shown in  
312 Clilverd et al. [1991] which were  $1400 \text{ el.cm}^{-3}$  and  $\sim 2800 \text{ el.cm}^{-3}$  respectively in June  
313 and December, at solar maximum. The 10-40% systematically higher results from the  
314 whistler-mode signals may be due to a slightly lower average L-shell than  $L=2.5$ , i.e.,  
315  $L=2.45$  [Saxton and Smith, 1989]. If the average whistler-mode L-shell used in  
316 Clilverd et al. [1991] is 0.05 L equatorward of  $L=2.5$  this would make only an 8%  
317 difference to the electron density calculations. The extrapolation error of 5% should  
318 also be included in this interpretation, suggesting that  $\sim 10\%$  of the difference between  
319 the two techniques could be due to errors in assumptions made. The remainder may be  
320 due to the requirement for whistler-mode signals to propagate in field-aligned electron  
321 density enhancements and suggest that duct enhancements maybe typically 20% of  
322 the average electron density levels, in agreement with previous ray-tracing  
323 calculations of 10-20% [Strangeways, 1991].

324

325 The change in the annual variation of  $N_{eq}$  with L-shell is shown in Figure 3 as a  
326 ratio of December to June  $N_{eq}$  values. Three longitudes are shown,  $+100^\circ$  (Asia),  $-60^\circ$

327 (America), and -150°(New Zealand). While not actually at the exact longitude of New  
328 Zealand, the longitude (-150°) is used because it is the appropriate longitude for the  
329 ‘New Zealand’ ground-based whistler-mode data [Clilverd et al., 1992] which showed  
330 an annual variation ratio of ~1.4. At Asian longitudes there is virtually no annual  
331 variation, with the Neq ratio staying within ±10% of unity. The American longitudes  
332 show a maximum ratio of 2.7 at L=2.5—3.5. By L=4.5 the annual variation in Neq  
333 has almost disappeared. The New Zealand longitudes show a relatively small annual  
334 variation, with a ratio of about 1.5, with a gradual decline in the effect with increasing  
335 L-shell.

336

337 The radial density profile in the plasmasphere is typically represented as an  $L^{-4}$   
338 distribution. The following expression based on the plasmaspheric model of Chappell  
339 et al. [1970] is used to represent the results obtained from whistler-mode signals:

340

$$341 \quad N_{eq} = 3877 P_e^2 [2/L]^N \quad \text{el.cm}^{-3} \quad (1)$$

342

343 where  $P_e$  is a plasma enhancement factor, usually taken as 1.0,  $N$  is the radial power  
344 law, usually assumed to be 4.0, and  $3877 \text{ el.cm}^{-3}$  is the electron density at  $L=2.0$ . The  
345 results of least squares fitting of equation (1) to the data for both +100°E (Asia) and -  
346 60°E (American) longitudes in December and June is shown in Figure 4. The values  
347 of  $P_e$  and  $N$  are shown in each panel, with the best fit represented by a solid line. The  
348 Neq data points are shown by diamonds. A dotted reference line using the empirical  
349 Carpenter and Anderson plasmasphere model [Carpenter and Anderson, 1992] for  
350 December and June during solar maximum conditions (sunspot number,  $R=150$ ) is  
351 also shown. The Carpenter and Anderson model was developed from satellite profiles

352 of  $N_{eq}$  that included coverage at  $L \leq 3$ , and restricted to those profiles where  $N_{eq} > 667$   
353  $\text{el.cm}^{-3}$  at  $L = 3$ . Profiles were then used until they became irregular at higher L-shells  
354 or exhibited a steeper negative slope. This, and the requirement that geomagnetic  
355 activity had been low for  $\sim 20$  hours prior to the profile measurement, ensured that the  
356 model represents the quiet-time, saturated plasmasphere. But the CRRES results  
357 shown in Figure 2 suggest that these electron density restriction at  $L = 3$  would reject  
358 some saturated plasmasphere conditions found at American longitudes around the  
359 time of the June solstice. We would expect our ECH limitation on the CRRES data  
360 selection to ensure saturated plasmasphere measurements, but potentially only at L-  
361 shells which are typically unaffected by weak or moderate geomagnetic activity ( $L <$   
362 4).

363

364 In Figure 4 the CRRES data for Asian longitudes ( $+100^\circ\text{E}$ ) show little variation  
365 with season, with  $P_e$  and  $N$  values very close to the normal values used, i.e., 1.0 and 4  
366 respectively. At American longitudes ( $-60^\circ\text{E}$ ) there are significant changes in the  
367 radial profile from December to June. In December the best fit is given by  $P_e=1.6$  and  
368  $N=5$ . So the  $L \leq 3$  density levels are elevated compared with normal values and the  
369 radial profile is steeper than expected. In June  $P_e=0.75$ , and  $N=3.4$  and the densities  
370 are lower than normal, and the radial profile is less steep. Averaged over longitude at  
371 any given time of year the density profiles should look similar to those given by  
372 Carpenter and Anderson, because their analysis did not take longitudinal variability  
373 into account. In practice this is true for our data until  $L > 3.5$ , after which the  
374 consistently lower densities seen in our data shows clear evidence that our analysis  
375 includes some non-saturated density levels, that would have been excluded from the  
376 Carpenter and Anderson model.

377

378 The annual variation in electron density should be mirrored in the ion density in  
379 order to conserve charge neutrality in the plasmasphere. In Figure 5 we plot the  
380 longitudinal and seasonal variation of  $\text{He}^+$  abundance derived from the IMAGE EUV  
381 experiment [Sandel et al., 2001]. The EUV units are  $\text{He}^+$  ( $\text{cm}^{-3}$ ), and are taken from  
382 measurements made in June and December 2001. The December EUV values are  
383 represented by crosses, with June values by diamonds. The longitudinal variations in  
384  $\text{He}^+$  closely match the electron density variations despite being taken from different  
385 solar cycles.

386

387 To avoid a bias introduced by the diurnal variation in ion abundance, we  
388 aimed to select times for which the phase of the magnetic longitude system was  
389 uniformly distributed in magnetic local time. The final set of images chosen was  
390 imperfect in this regard. Therefore we assessed the possibility that some of the  
391 structure in the EUV measurements in Figure 5 could arise from incomplete averaging  
392 of the diurnal variation over all magnetic longitudes. We created a simple model to  
393 compute the residual modulation in magnetic longitude that might result from our  
394 specific sampling of the diurnal variation. It showed a modulation of lower amplitude,  
395 having a shape different from the structure in Figure 5. We conclude that imperfect  
396 averaging of the diurnal variation does not significantly bias the structure measured in  
397 longitude.

398

399 Ion number densities have been calculated for Figure 5 using cross-phase analysis  
400 [Menk et al., 1999] for the longitudes of  $-65^\circ\text{E}$  and  $-10^\circ\text{E}$  at  $L=2.5$  for December/June  
401 2001. These data are shown in Figure 5 as squares (December) and triangles (June),

402 and also indicate a strong annual variation in density at the longitudes observed. The  
403 pair of magnetometer stations used for the  $-65^{\circ}\text{E}$  values is Millstone Hill and APL  
404 from the MEASURE array, and the  $-10^{\circ}\text{E}$  values are Hartland and York from the  
405 SAMNET array. Both midpoints are close to  $L=2.5$ , but have been normalised to  
406 exactly  $L=2.5$  assuming a radial  $L^{-4}$  variation. The ion values plotted at  $-65^{\circ}\text{E}$  have  
407 been adjusted by a factor of 1.3 in order to convert atomic mass units to number  
408 densities, and to make the plotted points match the electron densities at that longitude.  
409 The adjustment value suggests 11% composition of  $\text{He}^+$  and the EUV data suggest  
410  $\sim 20\%$ . These results are consistent with the  $\text{H}^+/\text{He}^+$  composition during quiet times.  
411 Environmental differences due to different sampling times, and differences due to  
412 different techniques may be adequate to account for the differences observed here.  
413 However, the ion values at  $-10^{\circ}\text{E}$  have been adjusted by a factor of 2.1. Although the  
414 data clearly shows the annual variation in density, the adjustment factor is much  
415 larger than expected and is consistent with significant heavy ion loading at these  
416 longitudes, i.e., about 6%  $\text{O}^+$ . However, this result is not inconsistent with the results  
417 from Sutcliffe et al. [1987] who found increasing plasma mass density with longitude  
418 eastwards towards  $20^{\circ}\text{E}$  in June at  $L\sim 1.78$ , due to increased  $\text{O}^+$  concentrations at 1000  
419 km, probably driven by vertical ion drifts from meridional winds in the upper  
420 ionosphere.

421

422 Implications for electron precipitation

423

424 The background electron density in the plasmasphere plays a key role in  
425 determining the resonant energy of wave-particle interactions. In this section we  
426 investigate the influence that the annual variation in electron density will have on

427 pitch-angle scattering of energetic electrons into the loss cone, out of the radiation  
428 belts, and subsequent precipitation into the atmosphere.

429

430 Meredith et al. [2006] calculated loss timescales for pitch angle scattering by  
431 plasmaspheric hiss using the PADIE code [Glauert and Horne, 2005] with wave  
432 properties based on CRRES observations. The determination of the diffusion  
433 coefficients requires knowledge of the distribution of the wave power spectral density  
434 with frequency and wave normal angle, together with the ratio  $f_p/f_{ce}$ , wave mode, and  
435 the number of resonances. The ratio  $f_{pe}/f_{ce}$  is dependent on the background electron  
436 density, and the background magnetic field.

437

438 Here we analyse the effect of differing levels of plasmaspheric density at  $L=3.0$  using  
439 the PADIE code. Following the analysis of Meredith et al. [2006] we use similar  
440 parameters to model the wave interactions. Since energetic outer zone electron loss  
441 timescales inside the plasmasphere can be explained by wave particle interactions  
442 with plasmaspheric hiss propagating at small or intermediate wave normal angles ( $\psi$ ),  
443 we assume a Gaussian angular spread in  $X$ , where  $X = \tan \psi$ , with a width  
444 corresponding to  $\psi = 20^\circ$ . Since wave propagation at an angle to  $B$  is included, we  
445 calculate the diffusion rates for Landau ( $n=0$ ) and  $\pm 10$  cyclotron harmonic resonances.  
446 We assume a wave power of  $900 \text{ pT}^2$  and that the wave spectra intensity peaks at  $0.55$   
447 kHz, with a bandwidth of  $0.3 \text{ kHz}$  and lower and upper cut-offs of  $0.1 \text{ kHz}$  and  $2.0$   
448 kHz respectively. Following Lyons et al. [1972] we calculate the bounce-averaged  
449 diffusion rate which takes into account the scattering of particles in pitch angle over  
450 the complete range of latitudes between the mirror points.

451

452 We use values of the ratio  $f_{pe}/f_{ce}$  that are equivalent to electron density levels of  
453  $1500 \text{ el.cm}^{-3}$  ( $f_{pe}/f_{ce}=10.8$ ),  $1000 \text{ el.cm}^{-3}$  ( $f_{pe}/f_{ce}=8.8$ ), and  $500 \text{ el.cm}^{-3}$  ( $f_{pe}/f_{ce}=6.2$ ).  
454 The PADIE code assumes a dipole magnetic field, and we use values of  $f_{pe}/f_{ce}$  that  
455 are calculated at the  $L=3.0$  geomagnetic equator. These density levels represent  
456 conditions at  $L=3.0$  for American longitudes in December ( $1500 \text{ el.cm}^{-3}$ ) and June  
457 ( $500 \text{ el.cm}^{-3}$ ) taken from Figure 2, and the Asian longitudes for most times of the year  
458 ( $1000 \text{ el.cm}^{-3}$ ). The pitch angle diffusion coefficients are shown in Figure 6. The  
459  $f_{pe}/f_{ce}$  conditions are shown, with the bounce-averaged diffusion coefficient ( $\langle D_{\alpha\alpha} \rangle$ )  
460 plotted against electron pitch angle for 3 different electron energies. At times the  
461 bounce-averaged diffusion coefficient becomes extremely small and lies off the plot  
462 for large ranges of pitch angle. The 100 keV results for pitch angles  $<65^\circ$  (long  
463 dashed line) during low plasmaspheric density conditions ( $f_{pe}/f_{ce}=6.2$ ) is an example.  
464 The plot shows that for 100 keV electrons the diffusion rate at the edge of the loss  
465 cone (vertical dot-dashed line at pitch angles of  $\sim 10^\circ$ ) is reduced by a factor of  $\sim 5$  as  
466 the plasmasphere becomes depleted to density levels equivalent of American  
467 longitudes around the June solstice. However, 1 MeV electron diffusion rates increase  
468 by a factor of  $\sim 3$ . Thus between December and June hiss driven precipitation into the  
469 atmosphere will become spectrally harder at American longitudes. At Asian  
470 longitudes, represented by  $f_{pe}/f_{ce}=8.8$ , there would be little change in the  
471 precipitation particle energy spectra with season since  $f_{pe}/f_{ce}$  hardly changes.

472

473 Discussion

474

475 Using CRRES observations set we have shown that the maximum amplitude of the  
476 annual variation in electron density is at American longitudes (about  $-60^\circ\text{E}$ ). This is in

477 good agreement with the analysis of Clilverd et al. [1991], and it seems very likely  
478 that this is primarily caused by the influence of the Earth's tilted-offset dipole  
479 magnetic field on the diffusive equilibrium conditions along the plasmaspheric field  
480 lines, as represented by Figure 1 of this paper. The annual variation has an amplitude  
481 of 2.7 at L=2.5 at solar maximum for American longitudes, which agrees with the  
482 corresponding densities derived from ground-based observations of whistler-mode  
483 signals. At New Zealand longitudes the ratio from CRRES observations was 1.5 for  
484 L=2.5, which is also very close to the value found from whistler-mode signals taken  
485 during the same period.

486

487 Several of the plasmaspheric models predicted that at Asian longitudes (+100°E) the  
488 June densities would exceed the December densities, by typically a ratio of 1.2  
489 [Guiter et al., 1995; Richards et al., 2000]. This result is not observed in the CRRES  
490 data, where the ratio is 1.0 at almost all of the L-shells at this longitude. Guiter et al.  
491 [1995] predicted that the December to June density ratio would increase slightly with  
492 increasing L-shell. This is not observed at any of the longitudes studied in detail.

493

494 The CRRES data shows that the June electron density levels at American longitudes  
495 are lower than for any other longitude. Clilverd et al. [1991] suggested that in June  
496 there would be very little longitudinal variation in electron density, and estimated  
497 Asian June density levels of  $1000 \text{ el.cm}^{-3}$ . This estimate was based on conjugate  
498 pairs of ionosonde data, since no suitable whistler-mode data was available for the  
499 Asian sector. For the African/Asian longitudes Nurmijarvi (60.5°N, 24.6°E) and  
500 Kerguelen (49.4°S, 70.2°E) were analysed – mainly because of the lack of choice of  
501 ionosonde stations in the southern hemisphere at these longitudes. These stations

502 represent L=3.0-3.5 conditions rather than L=2.5, and Figure 2 shows that typical  
503 Asian electron density levels at these L-shells of ~3.0 are ~1000 el.cm<sup>-3</sup>, thus  
504 explaining how the Asian sector equatorial electron density estimates of Clilverd et al.  
505 [1991] were too low. The longitudinal variation of Neq in June, although not  
506 previously predicted, is consistent with a tilted offset dipole magnetic field effect on  
507 plasmaspheric diffusive equilibrium conditions.

508

509 In Figure 4 we plotted the CRRES Neq results in comparison with the model of  
510 Carpenter and Anderson [1992] based on ISEE satellite data. The Carpenter and  
511 Anderson (C&A) model results for December at solar maximum agree reasonably  
512 well with the L=2.5-4.0 CRRES Neq at American longitudes (-60°E). At higher L-  
513 shells the CRRES satellite observes lower density levels than the C&A model; this  
514 may possibly be due to the CRRES data including unsaturated plasmasphere  
515 conditions. In June at American longitudes (-60°E) the C&A model over estimates the  
516 electron density level consistently at all L-shells, and in December L-shells greater  
517 than L=3.5 have consistently lower CRRES density levels than C&A. This appears to  
518 be in part because of the influence of some unsaturated plasmasphere Neq values in  
519 the CRRES data, and also because of the lack of a longitudinal component in the  
520 annual density variation of C&A.

521

522 Using the PADIE code and holding all variables constant apart from the background  
523 electron density we find that hiss driven precipitation into the atmosphere will become  
524 spectrally harder at American longitudes as the season changes from December to  
525 June. At Asian longitudes there would be little change in the precipitation particle  
526 energy spectra with season. An additional influence of the changing background

527 density in the plasmasphere could be on the generation and amplification of the hiss  
528 waves themselves. If the source of free energy to drive the waves remains the same,  
529 then reducing (increasing) the electron density should increase (decrease) the band of  
530 frequencies generated, affecting the resonant energies. So, although here we have  
531 shown that the annual changes in background electron density have an influence on  
532 the dynamics of radiation belt particles, the picture is far from complete and requires  
533 further study. Additionally, experimental evidence of this effect on the radiation belt  
534 particles has yet to be published.

535

536 Summary

537

538 We have used CRRES measurements of plasmaspheric equatorial electron density  
539 at solar maximum to investigate the longitudinal and annual variation in density in the  
540 range  $L=2.5-5.0$ . We find that the largest annual variation occurs at American  
541 longitudes ( $-60^\circ\text{E}$ ), and that no annual variation occurs at Asian longitudes ( $+100^\circ\text{E}$ ).  
542 These findings are in agreement with Clilverd et al. [1991]. The underlying cause is  
543 due to the influence of a tilted-offset dipole geomagnetic field. At American  
544 longitudes there is the largest discrepancy between geomagnetic latitude and  
545 geographic latitude. This leads to substantial annual variations in ionospheric plasma  
546 density, which map up into the plasmasphere as a consequence of diffusive  
547 equilibrium.

548

549 Plasmaspheric electron density is larger in December than in June in the region  
550 covering  $-180^\circ\text{E}$  to  $+20^\circ\text{E}$ . Elsewhere the ratio of December to June is very close to  
551 1.0. The annual variation also differs with L-shell. At American longitudes ( $-60^\circ\text{E}$ ),

552 and possibly at New Zealand longitudes, the maximum December/June ratio is at  
553  $L=2.5-3.5$ , with a value of 2.7 at American longitudes at solar maximum. At  $L=4.5$   
554 and above the annual variation disappears, possibly because the plasmasphere is not in  
555 diffusive equilibrium with the ionosphere at these high L-shells, or the inclusion of  
556 non-saturated electron density values from CRRES observations. The lowest electron  
557 density values for a given L-shell occur at American longitudes. This is particularly  
558 clear for the lower L-shells, although apparent as far out as  $L=4.5$ . These values occur  
559 in June. Clearly the plasmasphere is strongly controlled by the configuration of the  
560 Earth's magnetic field and the annual variations in the F2 regions that are in diffusive  
561 equilibrium with it.

562

563 Ion densities also show significant annual variations. There are similar longitudinal  
564 characteristics in the case of IMAGE EUV  $\text{He}^+$  measurements taken during June and  
565 December 2001. However, there are as yet unexplained differences in atomic mass  
566 density measurements calculated using the magnetometer cross-phase technique,  
567 where European values are significantly higher than those at American longitudes and  
568 require a large correction factor for the ion composition.

569

570 Calculations of the effect of changing plasmaspheric density on wave-particle  
571 interactions with plasmaspheric hiss indicate that the depletion of the plasmasphere at  
572 American longitudes in June results in a harder energy spectrum of electrons being  
573 precipitated into the atmosphere at those longitudes than anywhere else. Conversely,  
574 the softest energy spectrum occurs at the same longitudes in December. Little  
575 variation in precipitation energy spectrum is likely at Asian longitudes due to the  
576 absence of any significant annual variation in plasmaspheric density.

577

577

578 References

579

580 Anderson, R. R., D. A. Gurnett, D. I. Odem (1992), CRRES Plasma-Wave  
581 Experiment, *Journal Of Spacecraft And Rockets*, 29 (4), 570-573.

582

583 Berube, D., M. B. Moldwin, and J. M. Weygand (2003), An automated method for the  
584 detection of field line resonance frequencies using ground magnetometer techniques,  
585 *J. Geophys. Res.*, 108, 1348, doi:10.1029/2002JA009737.

586

587 Carpenter, D.L., and R.R. Anderson (1992), An ISEE/whistler model of equatorial  
588 electron-density in the magnetosphere, *J. Geophys. Res.*, 97, 1097-1108.

589

590 Chappell, C. R., K. K. Harris, G. W. Sharp (1970), Morphology of bulge region of  
591 plasmasphere, *J. Geophys. Res.*, 75 (19), 3848-3861.

592

593 Clilverd, M. A., A. J. Smith, and N. R. Thomson (1991), The annual variation in quiet  
594 time plasmaspheric electron density determined from whistler mode group delays,  
595 *Planet. Space Sci.*, 39, 1059-1067.

596

597 Clilverd, M. A., N. R. Thomson, and A. J. Smith (1992), Observation of two preferred  
598 propagation paths for VLF signals received at a non-conjugate location, *J. Atmos.*  
599 *Terr. Phys.*, 54, 1075-1079.

600

601 Clilverd, M. A., F. W. Menk, G. Milinevski, B. R. Sandel, J. Goldstein, B. W.  
602 Reinisch, C. R. Wilford, M. C. Rose, N. R. Thomson, K. H. Yearby, G. J. Bailey, I. R.  
603 Mann, and D. L. Carpenter (2003), In-situ and ground-based intercalibration  
604 measurements of plasma density at L=2.5, *J. Geophys. Res.*, 108,  
605 doi:10.1029/2003JA009866.  
606  
607 Gallagher, D. L., M. L. Adrian, and M. W. Liemohn (2005), Origin and evolution of  
608 deep plasmaspheric notches, *J. Geophys. Res.*, 110, A09201,  
609 doi:10.1029/2004JA010906.  
610  
611 Glauert, S. A., and R. B. Horne (2005), Calculation of pitch angle and energy  
612 diffusion coefficients with the PADIE code, *J. Geophys. Res.*, 110, A04206,  
613 doi:10.1029/2004JA010851.  
614  
615 Guiter, S. M., C. E. Rasmussen, T. I. Gombosi, J. J. Sojka, and R. W. Shunk (1995),  
616 What is the source of observed annual variations in plasmaspheric density, *J.*  
617 *Geophys. Res.*, 100, 8013-8020.  
618  
619 Gurnett, D. A., and R. R. Shaw (1973), Electromagnetic radiation trapped in the  
620 magnetosphere above the plasma frequency, *J. Geophys. Res.*, 78, 8136-8149.  
621  
622 Helliwell, R. A. (1965), *Whistlers and related ionospheric phenomena*, Stanford  
623 University Press, Stanford, California.  
624

625 Horne, R. B., S. A. Glauert, and R. M. Thorne (2003), Resonant diffusion of radiation  
626 belt electrons by whistler-mode chorus, *Geophys. Res. Lett.*, 30(9), 1493,  
627 doi:10.1029/2003GL016963.

628

629 Lyons, L. R., R. M. Thorne, and C. F. Kennel (1972), Pitch angle diffusion of  
630 radiation belt electrons within plasmasphere, *J. Geophys. Res.*, 77, 3455-3474.

631

632 Menk, F. W., D. Orr, M. A. Clilverd, A. J. Smith, C. L. Waters, and B. J. Fraser  
633 (1999), Monitoring spatial and temporal variations in the dayside plasmasphere using  
634 geomagnetic field line resonances, *J. Geophys. Res.*, 104, 19955-19970.

635

636 Menk, F. W., C. L. Waters, and B. J. Fraser (2000), Field line resonances and  
637 waveguide modes at low latitudes, 1. Observations, *J. Geophys. Res.*, 105, 7747-7761.

638

639 Meredith, N.P., R. B. Horne, R. M. Thorne, D. Summers, and R.R. Anderson (2004),  
640 Substorm dependence of plasmaspheric hiss, *J. Geophys. Res.*, 109, A06209,  
641 doi:1029/2004JA010387.

642

643 Meredith, N.P., R. B. Horne, S. A. Glauert, R. M. Thorne, D. Summers, J. M.  
644 Albert, and R.R. Anderson (2006), Energetic outer zone electron loss timescales  
645 during low geomagnetic activity, *J. Geophys. Res.*, 111, A05212,  
646 doi:10.1029/2005JA011516.

647

648 Olson, W. P., and K. Pfizter (1977), Magnetospheric magnetic field modelling,  
649 Annual Scientific Report, AFOSR Contract No. F44620-75-c-0033.  
650

651 Orr, D., and J. A. D. Matthew (1971), The variation of geomagnetic micropulsation  
652 periods with latitude and the plasmapause, *Planet. Space Sci.*, 19, 897-904.  
653

654 Park, C. G., D. L. Carpenter, and D. B. Wiggin, (1978), Electron density in the  
655 plasmasphere: whistler data on solar cycle, annual and diurnal variations, *J. Geophys.*  
656 *Res.*, 83, 3137-3144.  
657

658 Rasmussen, C. E., and R. W. Shunk (1990), A three-dimensional time-dependent  
659 model of the plasmasphere, *J. Geophys. Res.*, 95, 6133-6144.  
660

661 Richards, P. G., T. Chang, and R. H. Comfort (2000), On the causes of the annual  
662 variation in the plasmaspheric electron density, *J. Geophys. Res.*, 62, 935-946.  
663

664 Rippeth, Y., R. J. Moffett, and G. J. Bailey (1991), Model plasmasphere calculations  
665 for L-values near 2.5 at the longitude of Argentine Islands, Antarctica, *J. Atmos. Terr*  
666 *Phys.*, 53, 551-555.  
667

668 Rozanov, E., L. Callis, M. Schlesinger, F. Yang, N. Andronova, and V. Zubov (2005),  
669 Atmospheric response to NO<sub>y</sub> source due to energetic electron precipitation, *Geophys.*  
670 *Res. Lett.*, 32, L14811, doi:10.1029/2005GL023041.  
671

672 Sandel B.R., R.A. King, W.T. Forrester, D.L. Gallagher, A. L. Broadfoot, C.C. Curtis  
673 (2001), Initial results from the IMAGE extreme ultraviolet imager, *Geophys. Res.*  
674 *Lett.*, 28, 1439-1442.  
675

676 Sandel, B. R., J. Goldstein, D. L. Gallagher, and M. Spasojević (2003), Extreme  
677 ultraviolet imager observations of the structure and dynamics of the plasmasphere,  
678 *Space Sci. Rev.*, 109, 25-46.  
679

680 Saxton, J. M., and A. J. Smith (1989), Quiet time plasmaspheric electric fields and  
681 plasmasphere-ionosphere coupling fluxes at  $L = 2.5$ , *Planet. Space Sci.*, 37, 283-293.  
682

683 Singer, H. J., W. P. Sullivan, P. Anderson, F. Mozer, P. Harvey, J. Wygant, and W.  
684 McNeil (1992), Fluxgate magnetometer instrument on the CRRES, *J. Spacecr.*  
685 *Rockets*, 29, 599-601.  
686

687 Strangeways, H. J. (1991), The upper cutoff frequency of nose whistlers and  
688 implications for duct structure, *J. Atmos. Terr. Physics*, 53, 151-169.  
689

690 Sutcliffe, P. R., S. K. F. Hattingh, and H. F. V. Boshoff (1987), Longitudinal effects  
691 on the eigenfrequencies of low-latitude Pc3 pulsations, *J. Geophys. Res.*, 92, 2535-  
692 2543.  
693

694 Tarcsai, G., P. Szemeredy, and L. Hegymegi (1988), Average electron density profiles  
695 in the plasmasphere between  $L=1.4-3.2$  deduced from whistlers, *J. Atmos. Terr.*  
696 *Phys.*, 50, 607-611.

697

698 Taylor, J. P. H., and A. D. M. Walker (1984), Accurate approximate formulae for  
699 toroidal standing hydromagnetic oscillations in a dipolar geomagnetic field, *Planet.*  
700 *Space Sci.*, 32, 1119-1124.

701

702 Walker, A. D. M., J. M. Ruohoniemi, K. B. Baker, R. A. Greenwald, and J. C.  
703 Samson (1992), Spatial and temporal behaviour of ULF pulsations observed by the  
704 Goose Bay HF radar, *J. Geophys. Res.*, 97, 12187-12202.

705

706 Waters, C. L., F. W. Menk, and B. J. Faser (1994), Low latitude geomagnetic field  
707 line resonance; experiment and modelling, *J. Geophys. Res.*, 99, 17547-17558.

708

709 Webb, P. A., and E. A. Essex (2001), A dynamic diffusive equilibrium model of the  
710 ion densities along plasmaspheric magnetic flux tubes, *J. Atmos. Solar Terr. Phys.*,  
711 63, 1249-1260.

712

713 CLILVERD ET AL.: PLASMASPHERIC DENSITY VARIATIONS

714 Figure 1. The variation of the geographic latitudes of the footprints of the L=2.5 field  
715 line, showing significant changes in relative latitude in the longitude region of -60°E.  
716

717 Figure 2. The longitudinal variation of equatorial electron density from the CRRES  
718 data plotted for a range of L-shells. Data from the December solstice (solid lines) are  
719 compared with data from the June solstice (dashed line). An error bar is shown  
720 representing one standard deviation in the data.  
721

722 Figure 3. The variation of the December/June ratio with L-shell, at the longitudes of  
723 Asia, America, and New Zealand/Pacific, derived from the CRRES data.  
724

725 Figure 4. The radial profile of equatorial electron densities from CRRES data for a  
726 range of L-shells and longitudes (diamonds). Standard deviations for the data are  
727 shown. A fit to the data is given by the solid line, expressed in terms of  $P_e$  and  $N$  from  
728 equation (1). The Carpenter and Anderson (1992) model results for solar maximum  
729 conditions and low magnetic activity are also shown (dotted lines).  
730

731 Figure 5. The CRRES equatorial electron density variation with longitude at L=2.5 for  
732 December (solid line) and June (dashed line). The longitudinal variation of IMAGE  
733 EUV  $\text{He}^+$  abundances in 2001 for December (crosses) and June (diamonds) are shown  
734 in comparison, using the right-hand y-scale). Ion number densities from ground-based  
735 cross-phase techniques are shown for December (squares) 2003 and June 2001  
736 (triangles) using the atomic mass unit adjusted by a weighting factor – see text for  
737 more details.  
738

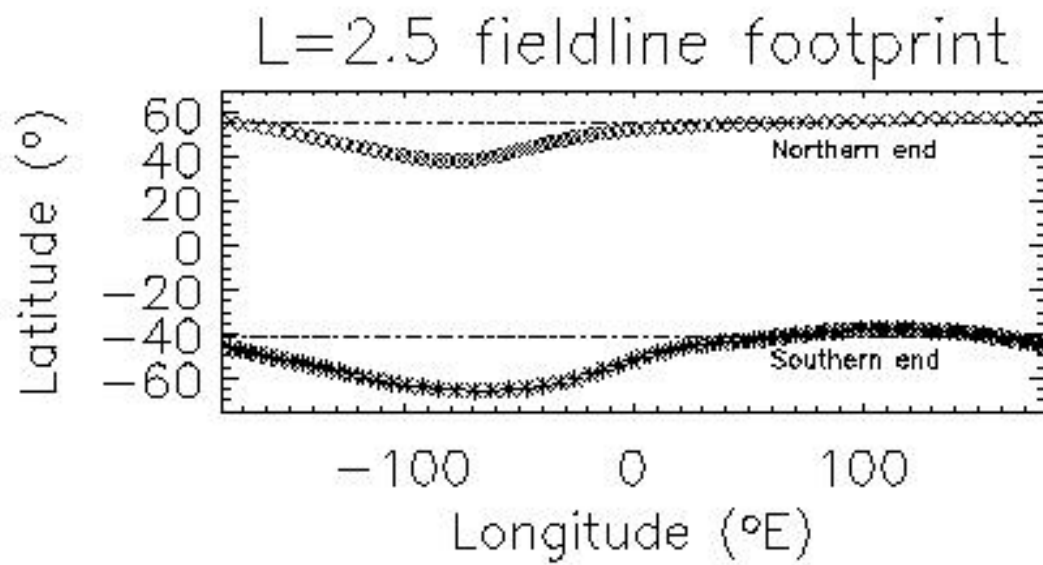
739

740 Figure 6. PADIE results for pitch angle diffusion coefficients at 100 keV, 300keV,  
741 and 1 MeV due to plasmaspheric hiss, for a range of plasmaspheric density conditions  
742 equivalent to density levels of  $1500 \text{ el.cm}^{-3}$  ( $f_{pe}/f_{ce}=10.8$ ),  $1000 \text{ el.cm}^{-3}$  ( $f_{pe}/f_{ce}=8.8$ ),  
743 and  $500 \text{ el.cm}^{-3}$  ( $f_{pe}/f_{ce}=6.2$ ) at  $L=3.0$ . The edge of the loss cone is indicated by a  
744 vertical dot-dashed line.

745

746

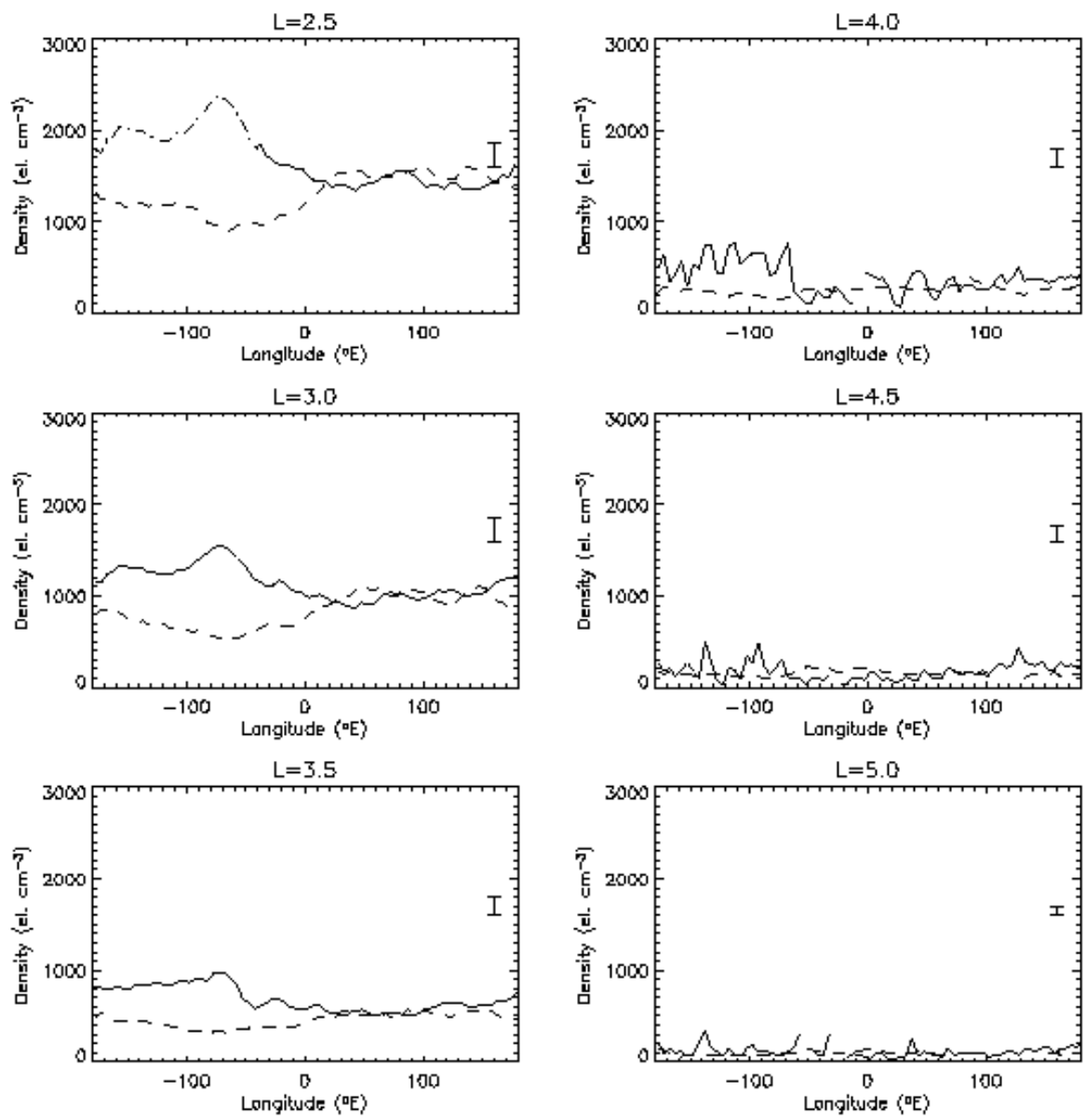
747



747

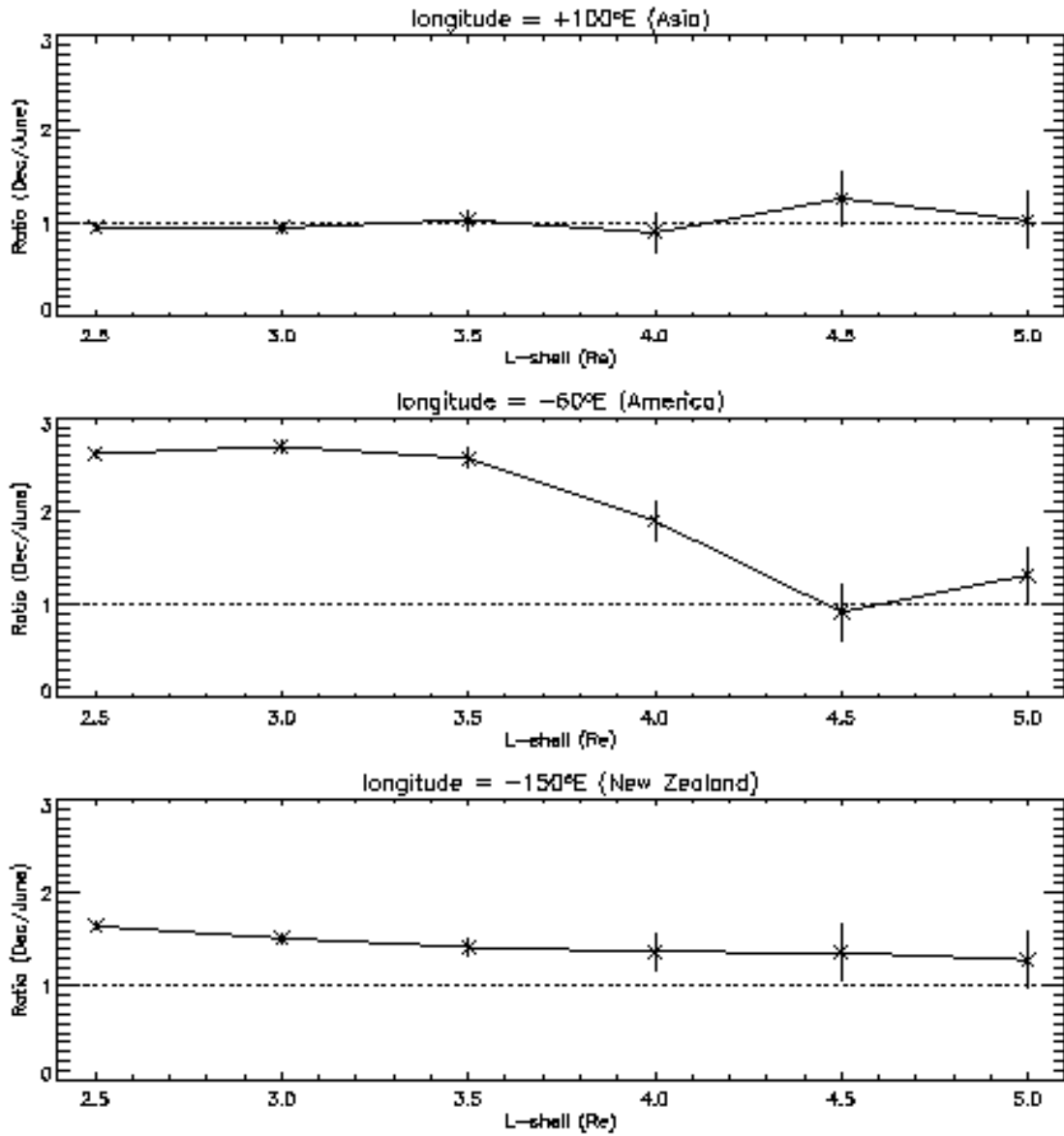
748 Figure 1. The variation of the geographic latitudes of the footprints of the L=2.5 field  
 749 line, showing significant changes in relative latitude in the longitude region of -60°E.  
 750

750  
751  
752



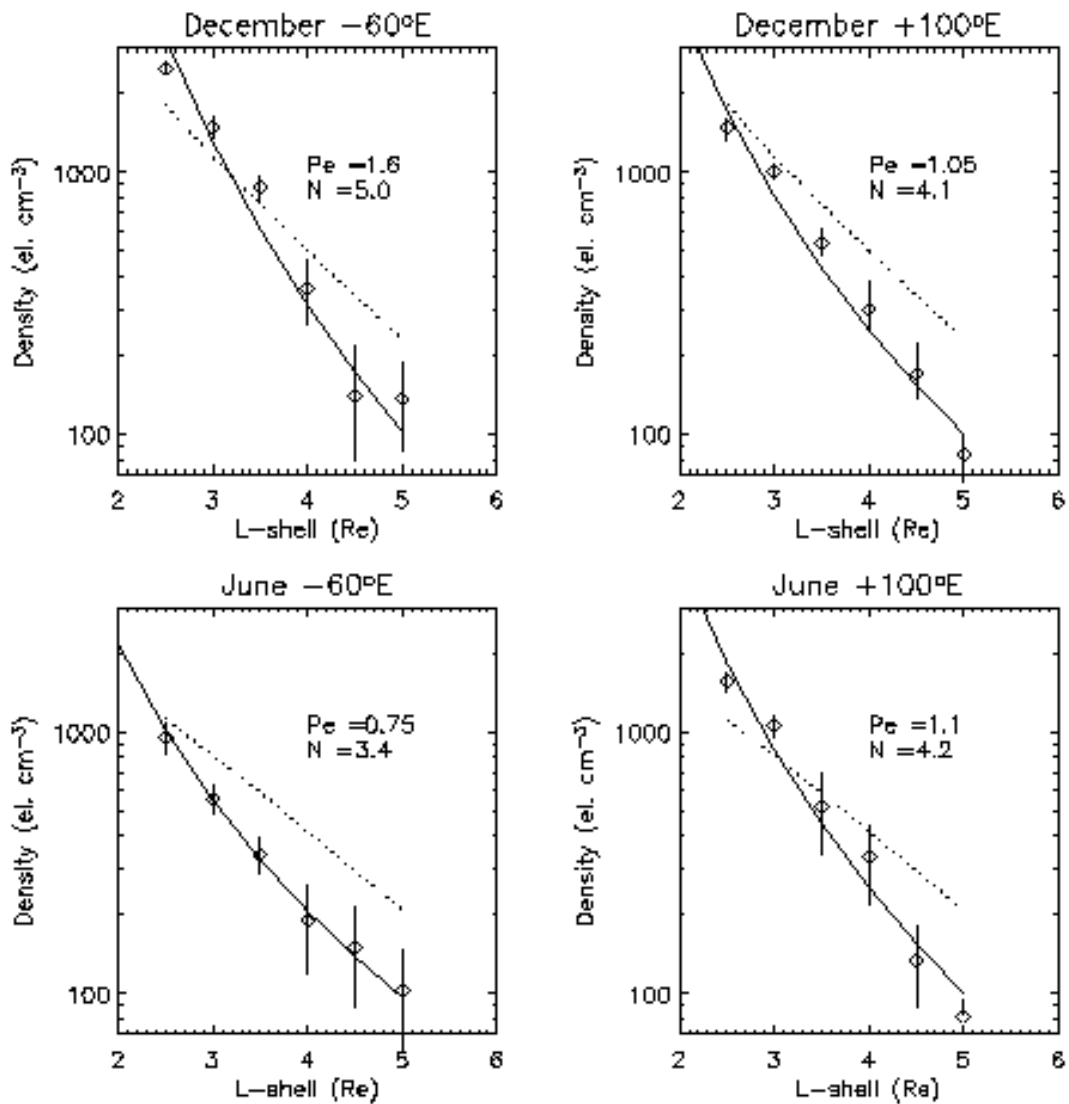
753  
754  
755  
756  
757  
758  
759

Figure 2. The longitudinal variation of equatorial electron density from the CRRES data plotted for a range of L-shells. Data from the December solstice (solid lines) are compared with data from the June solstice (dashed line). An error bar is shown representing one standard deviation in the data.



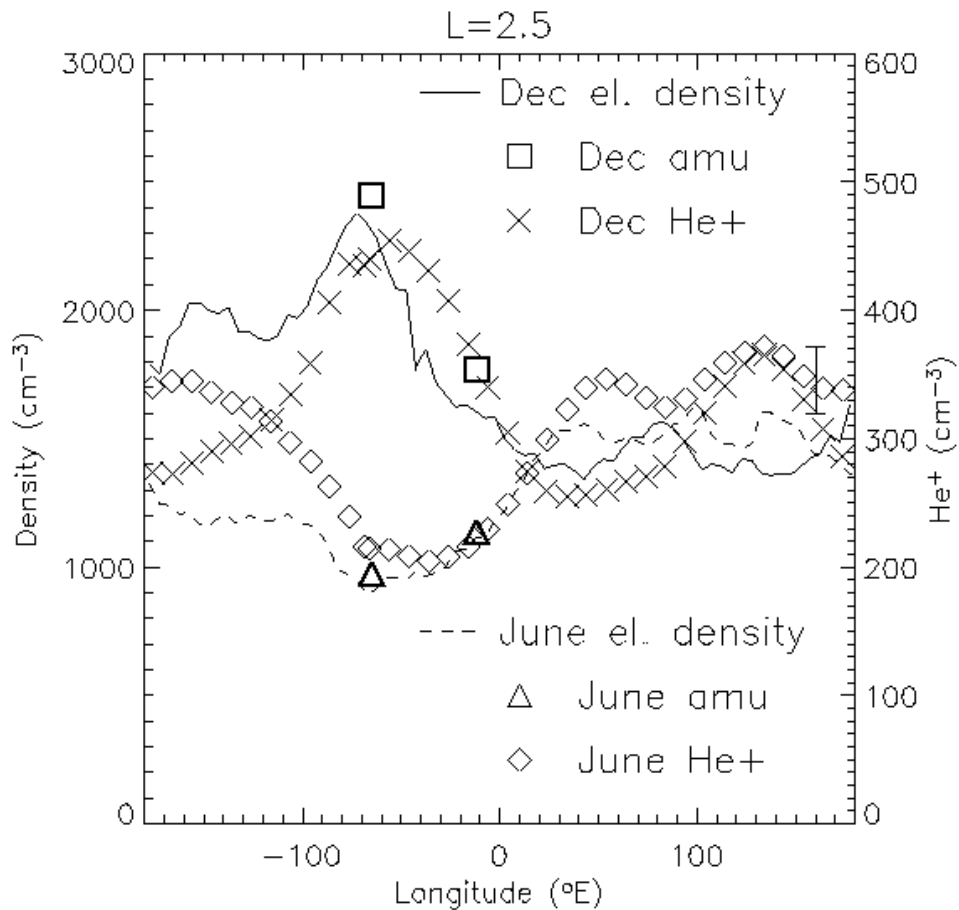
760  
 761  
 762  
 763  
 764  
 765

Figure 3. The variation of the December/June ratio with L-shell, at the longitudes of Asia, America, and New Zealand/Pacific, derived from the CRRES data.



766  
 767  
 768  
 769  
 770  
 771  
 772  
 773  
 774

Figure 4. The radial profile of equatorial electron densities from CRRES data for a range of L-shells and longitudes (diamonds). Standard deviations for the data are shown. A fit to the data is given by the solid line, expressed in terms of  $Pe$  and  $N$  from equation (1). The Carpenter and Anderson (1992) model results for solar maximum conditions and low magnetic activity are also shown (dotted lines).

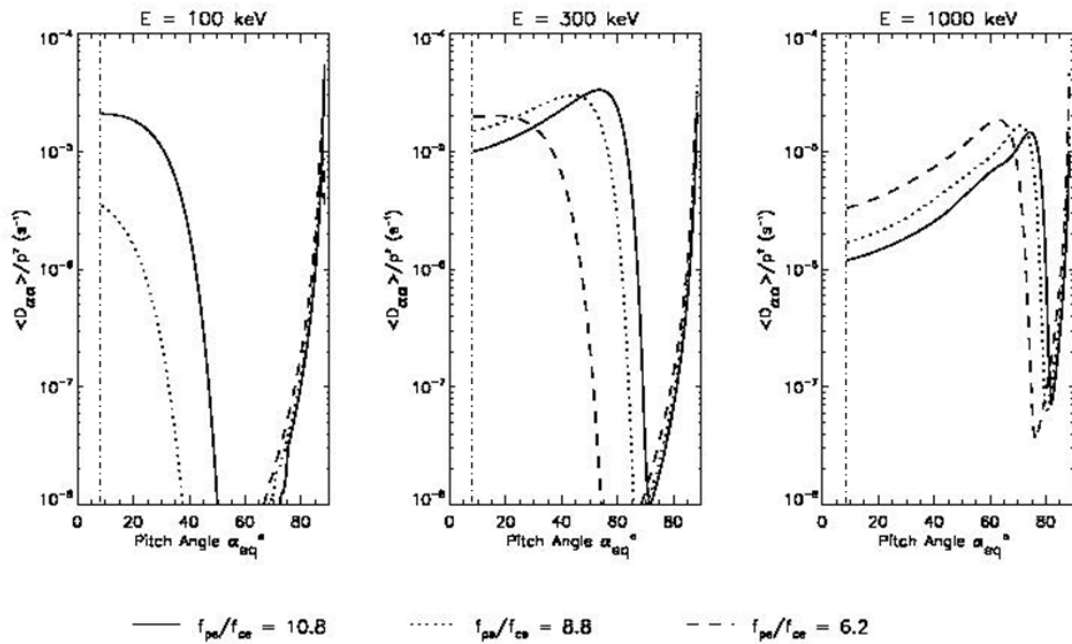


775

776

777 Figure 5. The CRRES equatorial electron density variation with longitude at L=2.5 for  
778 December (solid line) and June (dashed line). The longitudinal variation of IMAGE  
779 EUV He<sup>+</sup> abundances in 2001 for December (crosses) and June (diamonds) are shown  
780 in comparison, using the right-hand y-scale). Ion number densities from ground-based  
781 cross-phase techniques are shown for December (squares) 2003 and June 2001  
782 (triangles) using the atomic mass unit adjusted by a weighting factor – see text for  
783 more details.

784



785  
 786 Figure 6. PADIE results for electron pitch angle diffusion coefficients at 100 keV,  
 787 300keV, and 1 MeV due to plasmaspheric hiss, for a range of plasmaspheric density  
 788 conditions equivalent to density levels of  $1500 \text{ el.cm}^{-3}$  ( $f_{pe}/f_{ce}=10.8$ ),  $1000 \text{ el.cm}^{-3}$   
 789 ( $f_{pe}/f_{ce}=8.8$ ), and  $500 \text{ el.cm}^{-3}$  ( $f_{pe}/f_{ce}=6.2$ ) at  $L=3.0$ . The edge of the loss cone is  
 790 indicated by a vertical dot-dashed line.

791  
 792  
 793  
 794  
 795  
 796  
 797  
 798  
 799  
 800  
 801  
 802  
 803  
 804  
 805  
 806  
 807